Doppler solid flow measurement for chemical looping combustion

Fei Zhang,[1,2] D.W. Greve,[1,2] Fan Gao,[1,4] and I.J. Oppenheim[1,3]

[1]National Energy Technology Laboratory, Pittsburgh, PA, USA
[2]Department of Electrical and Computer Engineering, Carnegie Mellon University
[3]Department of Civil and Environmental Engineering, Carnegie Mellon University
[4]Department of Physics, Carnegie Mellon University, Pittsburgh, PA, USA

Introduction

Chemical looping combustion uses solid particles as an oxygen carrier for the combustion of coal. By using an oxygen carrier, the exhaust can be nearly pure carbon dioxide suitable for sequestration without the need for further separation. Measurement of the mass flow rate of the oxygen carrier particles in chemical looping combustion is important for process control. This is a challenging measurement problem because the particles are transported at high temperature (~900 °C) in an insulated duct. We report here on the development of a dual-frequency microwave Doppler sensor for this application.

Particle characteristics and scattering

In a chemical looping combustion system [1], oxygen carrier particles are saturated with oxygen in one reactor. These particles are transported to a combustion reactor where they react with gaseous or particulate fuel. When appropriately designed no nitrogen is transported into the combusion region, and consequently the exhaust is nearly pure carbon dioxide suitable for sequestration.

A wide variety of metal oxides have been considered for use as oxygen carriers for chemical looping combustion [2]. A particle diameter of 150 μm is typical and the particles are roughly spherical.

The scattering of electromagnetic waves from particles is most generally calculated using the Mie theory [3]. This theory is general and applies to both conducting and insulating particles of any size relative to the wavelength. When the wavelength λ is long enough in relation to the particle size the simpler Rayleigh expressions [3] can be used; the total scattering cross section $\sigma_{scattering,total}$ and the absorption cross section $\sigma_{absorption}$ are given by

$$\sigma_{scattering,total} = \frac{2}{3\pi}\frac{(2\pi r)^6}{\lambda^4}\left|\frac{m^2-1}{m^2+2}\right|^2 \quad \text{and} \quad \sigma_{absorption} = \frac{8\pi^2 r^3}{\lambda}\,\mathrm{Im}\left(\frac{m^2-1}{m^2+2}\right),$$

respectively, where *m* is the complex index of refraction of the particle and *a* is the radius. These expressions are valid provided $m \cdot 2\pi a/\lambda << 1$. For particles of the size typically used in chemical looping the Rayleigh expression is valid for frequencies in the 10-30 GHz range.

We consider here the specific characteristics of microwave scattering for ilmenite, one of many possible oxygen carriers. Ilmenite ($FeTiO_3$) has a relative dielectric permittivity of

approximately 6 and a finite electrical conductivity [4] at typical operating temperatures (~900 °C). **Figure 1** shows the predicted total scattering and absorption cross sections as a function of particle radius.

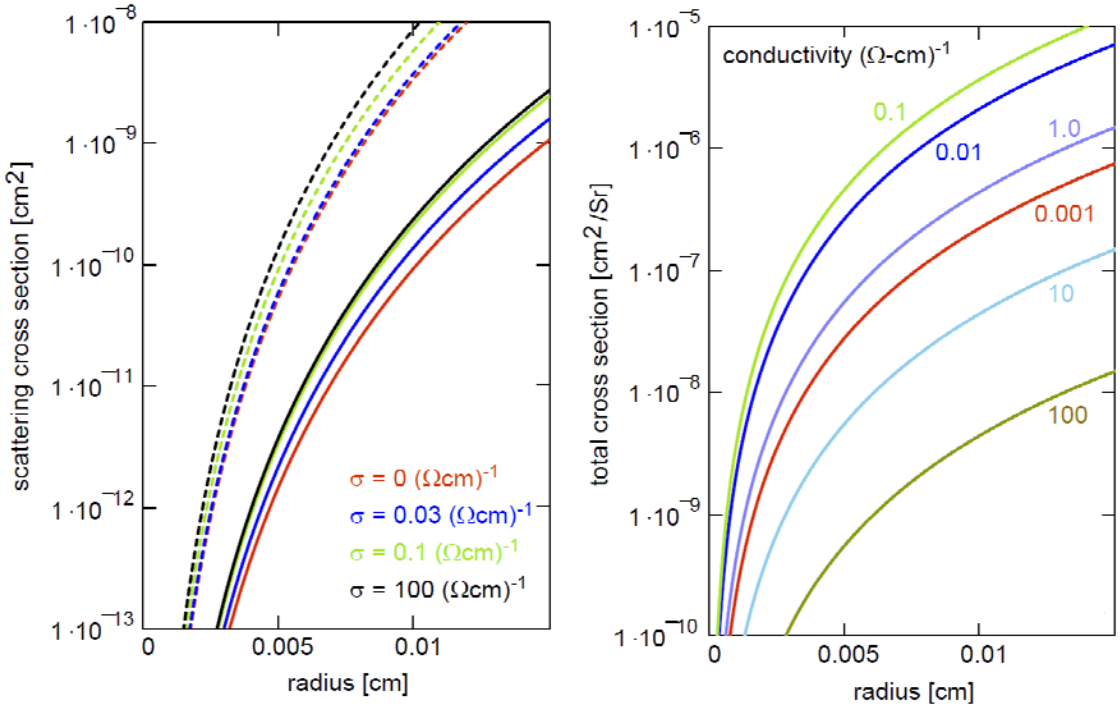

Figure 1. Predictions from the Rayleigh theory for scattering from spherical ilmenite particles. (Left) total scattering cross section as a function of particle size and electrical conductivity. Solid lines are for 10 GHz and dashed lines 24 GHz. (Right) absorption cross section at 10 GHz. The absorption cross section has a non-monotonic dependence on electrical conductivity.

Proposed configuration

Figure 2 shows the geometry of ports planned for Doppler flow sensing in the NETL chemical looping reactor. **Figure 2**a shows the inside diameter of the flow region. Because the system operates near 900 °C the flow region is surrounded by insulation with varying thickness. The Doppler sensor is to be located at the top in the "crossover" region where oxygen carriers are transported to the fuel reactor. The insulation at this point is approximately 13 cm in thickness. Ports for the flow sensor are oriented as shown in the detail drawing (**Figure 2**b). The microwave energy will be transported to the flow region in an alumina cylinder 2.54 cm in diameter which acts as a dielectric waveguide and also provides for a pressure seal between the flow region and the atmosphere. The alumina is surrounded by a steel tube where it enters the reactor and extends through a thick layer of insulation. The reactor has been built and is now being brought into operation. The microwave Doppler sensor is being developed and tested in a room temperature environment and will be installed in the reactor when completed. **Figure 2**c shows the block diagram for the microwave Doppler electronics. The oscillator signal is directed to a circulator and is then emitted from a horn antenna. The Doppler-shifted signal reflected

from moving objects is circulated to the intput of a mixer. Upon mixing with the attenuated oscillator signal, the time-dependent output contains both sum and difference frequencies. The sum frequency is removed by the low-pass filter and the remaining signal is digitized for later analysis. In the interests of experimental flexibility, this is constructed using individual components interconnected using coaxial cables.

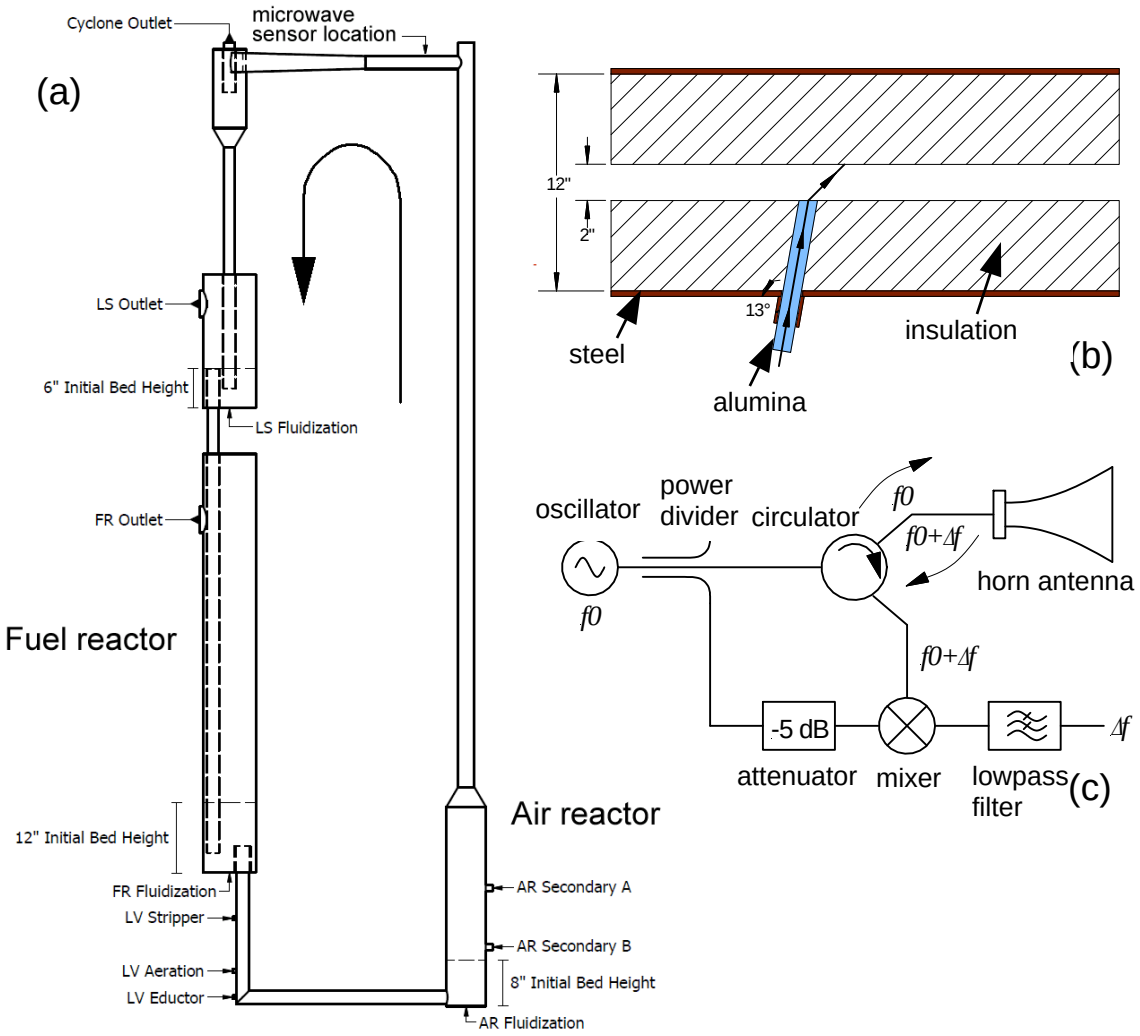

Figure 2. The Doppler flow sensor: (a) outline drawing of the NETL cold flow reactor showing the sensor location; (b) detail drawing showing the insulation around the flow region and the microwave launcher; and (c) block diagram of the microwave circuit.

Room-temperature tests

In order to verify operation of the electronics, we have tested the 10 GHz electronics at room temperature. Experiments have been performed using either single steel balls or flows of ilmenite particles 150 μm in diameter. A vertically oriented drop tube approximately 2 m in length was used, with either single ball drops or an ilmenite flow produced by a table feeder. A horn antenna was placed about 1.8 m from the top of the drop tube, 18 cm from the centerline of the drop tube and oriented downwards. After low-pass filtering the output of the mixer was digitized by a National Instruments USB-

6212 data acquisition unit. For testing purposes, we use a Labview application to record several seconds of data at a rate of 10,000 samples/ second. The Doppler frequency shift for the velocities of interest is of the order of hundreds of Hz, so this sampling rate is well above the Nyquist rate. The records are then analyzed off-line.

Figure 3 shows typical records obtained for a single ball drop (**Figure 3**a) and during a flow of approximately 73 gm/ sec[1] of ilmenite particles (**Figure 3**b). For a single ball the signal is approximately a windowed chirp signal. Based on the theory of the Doppler effect we expect the reflected signal to be frequency-shifted by $\Delta f = 2 f (v / c) \cdot \cos\theta$ where f is the frequency of the incident wave, v is the velocity of the reflecting particle, c the velocity of light, and θ the angle between the incident beam and the particle velocity. In our configuration with the horn pointing along the direction of fall the angle is smallest when the ball enters the illuminated region, and greatest when leaving. Consequently the chirp is from low to high frequency. The Fourier power spectrum of this signal shows a peak at about 310 Hz (**Figure 4**a). This corresponds to a velocity of 600 cm/sec, in good agreement with the theoretical velocity of 640 cm/sec for a 1.8 m drop when friction is neglected.

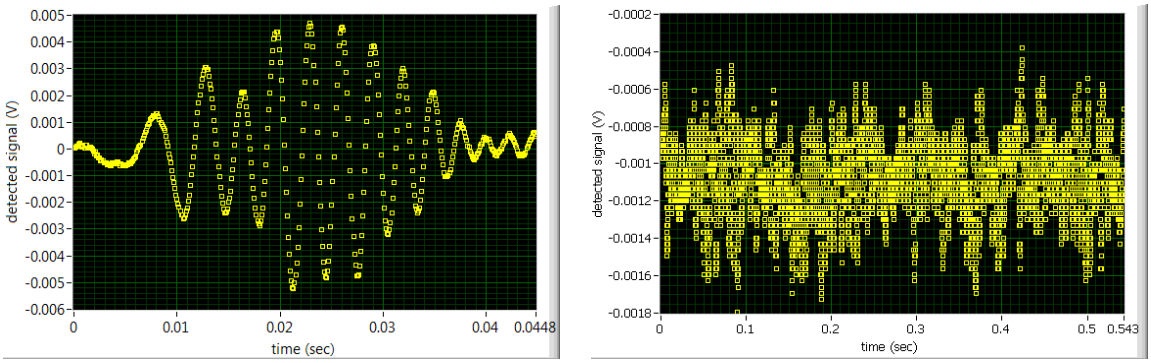

Figure 3. Mixer output signal as a function of time: (left) steel ball 0.157" diameter falling 1.8 m, horn angle 42°; (right) ilmenite from table feeder falling 2.1 m, angle 52°.

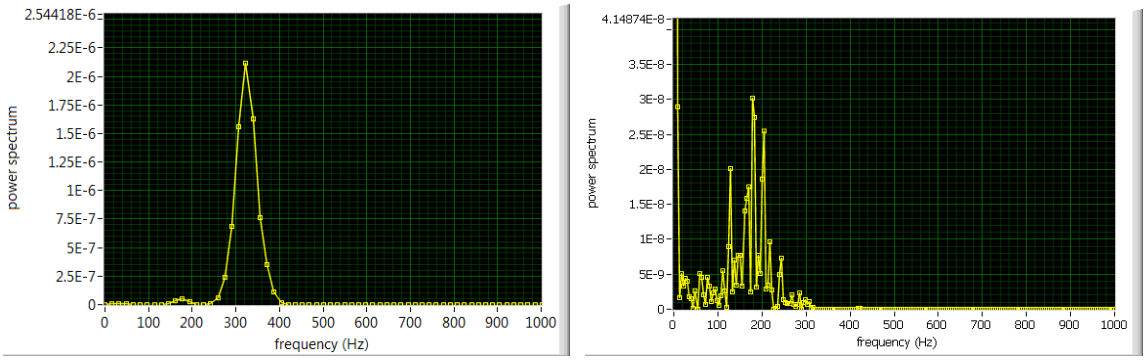

Figure 4. Fourier power spectrum calculated from mixer output signal: (left) 0.157" diameter steel ball, and (right) ilmenite from table feeder.

[1] The flow from the table feeder is high when first turned on and then remains approximately constant until all the material in the feeder is consumed. The flow rate was calculated by dividing the total mass in the feeder by the total flow time; consequently the flow after the start is somewhat less than 73 gm/ sec.

Figure 3 (right) shows the signal recorded for approximately 0.5 seconds of a nearly constant ilmenite flow. Note that this duration of this signal is substantially longer than **Figure 3**a. This signal is the superposition of signals from a very large number ($\sim 3 \times 10^5$) particles. The envelope of the Fourier power spectrum (**Figure 4**b) is distinctly peaked but has a spiky appearance. This is a consequence of the way in which the contributions from the many individual scattering particles add up. Note that the peak of the envelope is at a somewhat lower frequency (~190 Hz). The corresponding average velocity is 460 cm/sec, somewhat less than the velocity in the absence of air scattering but greater than the terminal velocity of a single 150 μm ilmenite particle in air. For approximately double the flow rate of ilmenite the velocity is essentially the same and the peak height in the Fourier power spectrum increases roughly proportionally to the flow rate (not shown). These results demonstrate the expected behavior and adequate sensitivity for measurement of the flows of interest. In operation the sensor will provide outputs for the measured velocity (from the frequency shift) and mass density (from the magnitude of the scattered signal).

Microwave launcher design

A crucial part of the sensor design is the development of a microwave launcher that meets the specific requirements of this application. In particular, the launcher must tolerate the high temperatures in the reactor and must not cause significant flow disturbance. An early decision was made to use a 2.54 cm cylindrical alumina waveguide terminating at the flow region and extending through the outer housing and insulation. Given the alumina relative dielectric permittivity of about 9, there are several wavelengths across the waveguide even at the lower operating frequency of 10 GHz. It was therefore anticipated that Snell's law would cause a bend in the propagation direction at the alumina-air interface (Fig. 2b). An angle of 77 degrees with respect to the flow direction was chosen, which according to Snell's law should give an angle of propagation of approximately 45 degrees in the flow region. Here we report the results of electromagnetic field simulations of the launcher with this geometry.

We consider first launching a wave into the alumina cylinder from a coaxial input. Simulations were performed using the emw mode of COMSOL 4.2a. We wish to launch the TE_{11} mode which has nearly uniform electric and magnetic fields across the cylinder and should therefore couple efficiently to a plane wave in air. At 10 GHz an alumina waveguide 2.54 cm in diameter is overmoded, with numerous other modes above cutoff (up to TE_{61} and TM_{41}). Commercial coaxial to circular waveguide transitions are available [5] and the problem of launching the TE_{11} mode into an overmoded waveguide has been considered in the literature [6]. However in most applications the waveguides are sized so that only a few additional modes can propagate. In our case short probes inserted into the cylinder from either the side or the end tend to excite modes other than the TE_{11}. Figure 5 shows one example of waves excited by an end probe. In this case the TM_{01} mode is strongly excited and S_{11} = -12.8 dB for the optimal probe length and location.

Considerably better results were obtained using a coaxial to rectangular waveguide transition followed by a tapered alumina section to make a transition from the rectangular waveguide to the circular launcher. The coaxial to rectangular waveguide section is filled

with alumina and is therefore much smaller than usual for a 10 GHz transition. **Figure 6** (right) shows the geometry that was simulated.

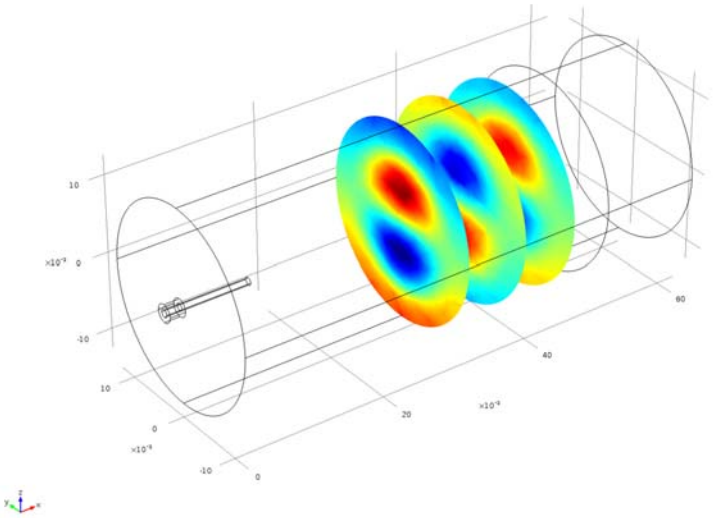

Figure 5. Excitation of a circular waveguide with a small end probe. The color indicates the H_y component.

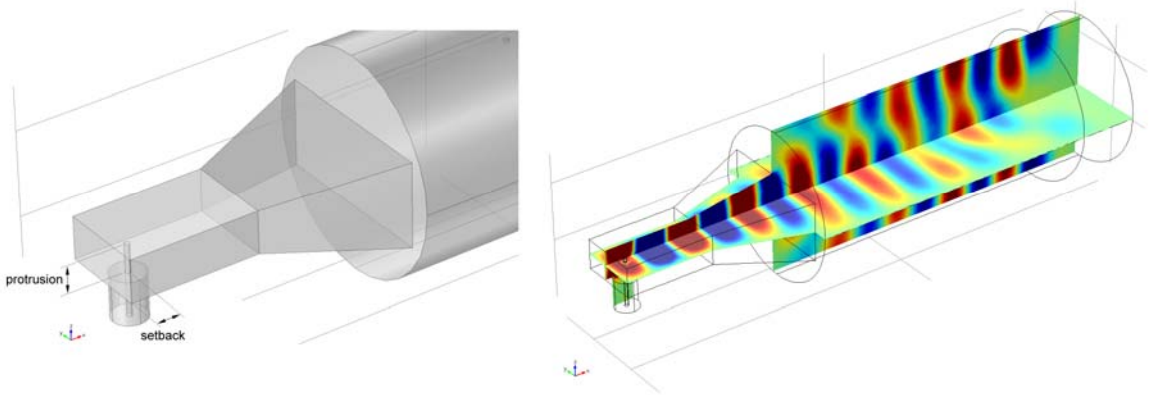

Figure 6. Geometry of the tapered coaxial to circular waveguide transition (left) and simulated *x* component of the electric field (right).

Figure 7 (left) shows the simulated S_{11} for this geometry as a function of the protrusion of the coaxial probe and the spacing of the probe from the back wall as defined in **Figure 6**(left). A minimum value of $S_{11} \approx$ -29 dB is obtained for the optimal values of the protrusion and setback. **Figure 6** (right) shows the *z* component of the electric field for these optimum values. A nearly planar wavefront with uniform electric field is obtained as desired for the TE_{11} mode.

We now consider launching of the TE_{11} mode from the alumina cylinder into air. We simulated an alumina cylinder about 5 cm long angled at 77 degrees and launching a wave into a half-sphere of air with 9 cm radius (**Figure 7**). The half-sphere is surrounded by a perfectly matched layer to absorb the emitted electromagnetic wave. A port boundary condition is defined at the end of the alumina cylinder and boundary mode analysis is performed prior to solving the field equations.

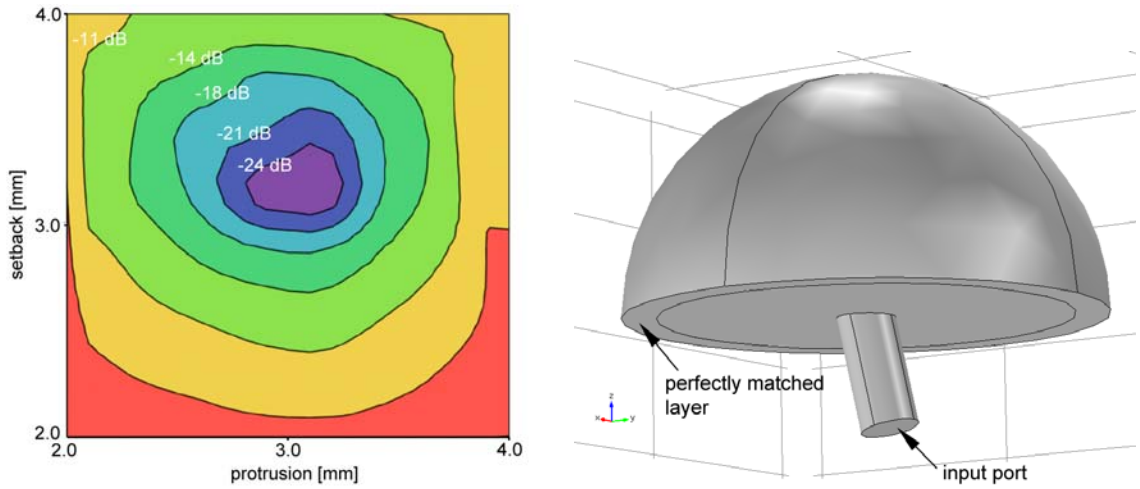

Figure 7. (Left) S_{11} as a function of probe protrusion and spacing from the back wall for the tapered coaxial to waveguide transition; and (right) geometry for simulating launch of microwaves into air from an alumina cylinder.

Figure 8 shows the results from simulations of the launched wave at 10 GHz. The mode resulting from the boundary mode calculation has a wavenumber of 6.11 cm^{-1}, close to the wavenumber for the TE_{11} mode in alumina. The electric field in the direction normal to the surface is plotted in **Figure 8** (right) and the time-averaged energy density contours are plotted in **Figure 8** (left). The microwave energy density is highest at an angle near 45 degrees, as expected. From the reflected power we calculate S_{11} = -12.5 dB at the input port.

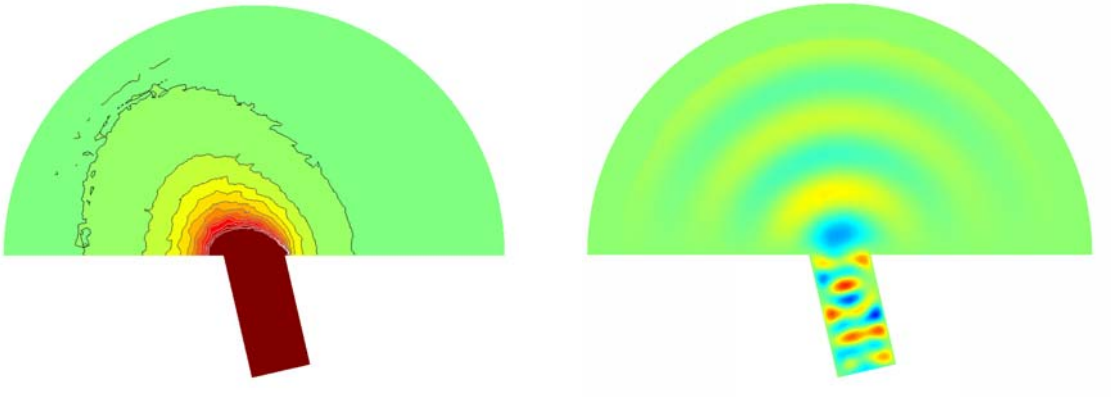

Figure 8. Results of simulation of microwave launch from alumina cylinder into air: (left) contours of constant time-averaged energy density and (right) electric field normal to the surface.

Summary

We have reported our progress toward the development of a microwave Doppler flow sensor for chemical looping combustion systems. Relevant cross sections for absorption and scattering have been calculated using the Rayleigh scattering theory. An initial demonstration of Doppler measurements on an ilmenite particle flow has been completed.

Design and simulation of a microwave launcher suitable for incorporation into the NETL cold flow reactor has also been reported.

Acknowledgements

As part of the National Energy Technology Laboratory's Regional University Alliance (NETL-RUA), a collaborative initiative of the NETL, this technical effort was performed under the RES contract DE-FE0004000. This project was funded by the Department of Energy, National Energy Technology Laboratory, an agency of the United States Government, through a support contract with URS Energy &Construction, Inc. Neither the United States Government nor any agency thereof, nor any of their employees, nor URS Energy & Construction, Inc., nor any of their employees, makes any warranty, expressed or implied, or assumes any legal liability or responsibility for the accuracy, completeness, or usefulness of any information, apparatus, product, or process disclosed, or represents that its use would not infringe privately owned rights. Reference herein to any specific commercial product, process, or service by trade name, trademark, manufacturer, or otherwise, does not necessarily constitute or imply its endorsement, recommendation, or favoring by the United States Government or any agency thereof. The views and opinions of authors expressed herein do not necessarily state or reflect those of the United States Government or any agency thereof.

References

1. B. Kronberger, C. Beal, J.-X. Morin, H. Hofbauer, "Design, hydrodynamic testing and scale-up recommendations of a conceptual large-scale chemical-looping combustion power plant," DOE NETL Conference, Washington DC, USA, (May 2004).

2. Lyngfelt, A., Kronberger, B., Adanez, J., Morin, J.-X., and Hurst, P., The GRACE project. Development of oxygen carrier particles for chemical-looping combustion. Design and operation of a 10 kW chemical-looping combustor. *Greenhouse Gas Control Technologies* **7** (2005) 115-123 (7*th International Conference on Greenhouse Gas Control Technologies*, Vancouver, Canada, 5^{th}-9^{th} September 2004).

3. Handbook of Surface and Colloid Chemistry, Third Edition, pp. 722-723, Chapter 19, C.M. Sorenson, *Handbook of Surface and Colloid Chemistry*, Third Edition, edited by K. S. Birdi, pp. 719–745 (CRC Press, 2008).

4. B. Zhang, T. Katsura, A. Shatskiy, T. Matsuzaki, and X. Wu, "Electrical conductivity of $FeTiO_3$ ilmenite at high temperature and high pressure," Physical review B **73**, 134104 (2006).

5. Microwave Engineering Corporation, North Andover, MA.

6. M.D. Desphande and B.N. Das, "Analysis of an end launcher for a circular cylindrical waveguide," IEEE Trans. Microwave Theory and Techniques MTT-26, 672 (1978).